BIOCHEMISTRY
including biophysical chemistry & molecular biology

Article

pubs.acs.org/biochemistry

Mapping Unstructured Regions and Synergistic Folding in Intrinsically Disordered Proteins with Amide H/D Exchange Mass Spectrometry

Theodore R. Keppel,[†,‡] Brent A. Howard,[†] and David D. Weis*[,†,‡]

[†]Department of Chemistry and [‡]Ralph N. Adams Institute for Bioanalytical Chemistry, University of Kansas, 1251 Wescoe Hall Drive, Lawrence, Kansas 66045, United States

Supporting Information

ABSTRACT: Mapping the structured and disordered regions and identifying disorder-to-order transitions are essential to understanding intrinsically disordered proteins (IDPs). One technique that can provide such information is H/D exchange coupled with mass spectrometry (H/D-MS). To explore the feasibility of H/D-MS for mapping disordered and ordered regions in IDPs, we undertook a systematic evaluation of an unstructured protein, a molten globular protein, and the well-folded complex of the two proteins. Most segments of the unstructured protein, ACTR (activator of thyroid and retinoid receptors, NCOA3_HUMAN, residues 1018−1088), exchange at rates consistent with its assignment as an unstructured protein, but there is slight protection in regions that become helical in the ACTR−CBP complex. The molten globular protein, CBP (the nuclear coactivator binding domain of the CREB binding protein, CBP_MOUSE, residues 2059−2117), is moderately protected from exchange, and the protection is nearly uniform across the length of the protein. The uniformity arises because of rapid interconversion between an ensemble of folded conformers and an ensemble of unstructured conformers. Rapid interconversion causes the H/D exchange kinetics to be dominated by exchange by molecules in unstructured conformations. For the folded ACTR−CBP complex, the exchange data provide a qualitatively accurate description of the complex. Our results provide a useful framework to use in the interpretation of H/D-MS data of intrinsically disordered proteins.

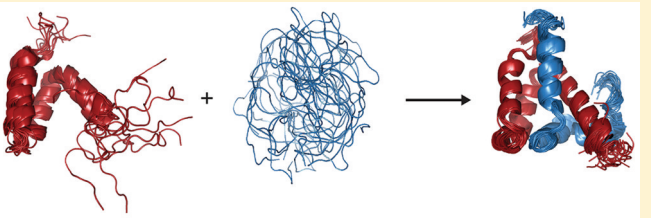

Intrinsically disordered proteins (IDPs) contain one or more regions that exhibit a high degree of conformational flexibility and lack a structured conformation. Many IDPs use disordered regions to carry out function.[1−11] IDPs differ from structured proteins by having a low level of sequence complexity and a bias against hydrophobic residues; these differences have become the basis of a variety of algorithms for predicting disorder.[12] Disorder prediction algorithms have shown that IDPs are ubiquitous in the proteomes of higher organisms and comprise roughly one-third of all proteins.[13,14] Bioinformatic approaches have demonstrated a clear distinction between the functions of structured proteins and disordered proteins. While protein structure is associated primarily with functions such as enzyme catalysis, ion channels, and cellular structure, protein disorder is associated primarily with functions that require protein−protein interactions such as signaling.[14]

In many cases, the disordered regions that mediate protein−protein interactions undergo coupled binding and folding.[15,16] There has been speculation that the affinity of many IDP-mediated protein−protein interactions is significantly decreased by the strong entropic driving force for the free unstructured protein.[8] At the same time, the conformational flexibility of the unstructured protein allows it to sample many different conformational states. Higher chain flexibility also produces greater binding rates in IDPs because of a larger target capture radius in solution.[17] Low affinity, coupled with high specificity, is an essential element for the transient protein−protein interactions required in cellular signaling. In many cases, a single disordered protein can recognize many different binding partners with the same disordered region, often adopting different folds upon binding.[18] Understanding the mechanisms of disorder-mediated protein interactions requires information about the unstructured regions of the proteins and their disorder-to-order transitions.

Many different experimental techniques for characterizing disordered proteins are available.[19−21] The techniques can be divided into those that provide only a global picture of the extent of disorder (e.g., size exclusion chromatography, intrinsic fluorescence, circular dichroism, small-angle X-ray scattering, and atomic force microscopy) and a more limited list of those that provide localized to atomic-scale resolution (e.g., NMR, limited proteolysis, and fluorescence resonance energy transfer). To map regions of a protein that undergo coupled binding and folding, localized information is essential. One technique that can provide such information is amide H/D exchange. Amide hydrogens, along the protein backbone, are susceptible

Received: February 14, 2011
Revised: September 2, 2011
Published: September 6, 2011

dx.doi.org/10.1021/bi200875p | *Biochemistry* 2011, 50, 8722−8732

to exchange with deuterium from D_2O because of dynamic fluctuations that disrupt amide hydrogen bonding.[22−24] By dilution of a protein with a large excess of D_2O, amide H/D exchange can be used as a probe of backbone flexibility. By measuring the rate at which deuterium is incorporated, we can determine the relative flexibility of different backbone segments. When H/D exchange is measured by NMR,[25,26] by mass spectrometry of proteolytic fragments,[27] or by a top-down fragmentation MS approach,[28] one can obtain localized information about the backbone flexibility of the protein of interest. The MS approach offers several advantages, including the ability to work with large proteins at low protein concentrations in physiological buffers and the ability to detect all proteins in a complex without selective isotopic labeling.

There are many examples of flexible segments in otherwise well-folded proteins identified by H/D-MS (see, for example, refs 29 and 30). The technique has also been used to characterize chemically unfolded proteins,[31,32] yet the use of H/D-MS to obtain local flexibility data on IDPs is considerably more limited.[33−35] To establish the utility of segment-averaged H/D exchange MS measurements for the characterization of IDPs and their interactions, we have undertaken a study of two model IDPs representing the extremes of the disorder spectrum: ACTR, the unstructured activation domain of the activator of thyroid and retinoid receptors (NCOA3_HUMAN, residues 1018−1088), and CBP, the molten globular nuclear coactivator binding domain of the CREB binding protein (CBP_MOUSE, residues 2059−2117). Here, we have used isolated CBP and ACTR and their complex[15] as model systems to explore the capability of H/D-MS to characterize intrinsically disordered proteins and coupled binding and folding.

MATERIALS AND METHODS

Materials. Ampicillin and isopropyl β-D-1-thiogalactopyranoside (IPTG) were obtained from Research Products International Corp. (Mt. Prospect, IL). LB medium used for cell cultures was prepared with Bacto Tryptone and Bacto Yeast Extract obtained from Becton, Dickinson, and Company (Franklin Lakes, NJ). Pepsin from porcine gastric mucosa, piperazine, sodium hydroxide, DL-dithiothreitol, bestatin hydrochloride, E-64, 4-(2-aminoethyl)benzenesulfonyl fluoride hydrochloride (AEBSF), pepstatin A2, and deuterium oxide (99.9% D) were obtained from Sigma (St. Louis, MO). Benzonase nuclease was obtained from EMD Chemicals (Gibbstown, NJ). Formic acid (>99%), used as an additive in prepared mobile phases, was obtained from Thermo Scientific (West Palm Beach, FL). Sodium phosphate monobasic, sodium phosphate dibasic, sodium hydroxide hydrochloric acid, boric acid, Tris base, and sodium chloride were obtained from Fisher Scientific (Hanover Park, IL). Optima LC−MS grade acetonitrile and water used in chromatography were both obtained from Fisher Scientific. POROS 20 AL column packing material was obtained from Applied Biosystems (Carlsbad, CA).

Protein Expression. CBP and ACTR domains were coexpressed from a pET22B coexpression vector[15] in *Escherichia coli* strain BL21 Star(DE3) (Invitrogen, Carlsbad, CA). The glycerol stock was streaked onto agar plates containing 0.1 g/L ampicillin and grown overnight at 37 °C. All cell cultures were grown in LB medium [10 g/L tryptone, 5 g/L yeast extract, and 10 g/L NaCl (pH 7.0)] containing 0.1 g/L ampicillin. Cells were grown at 37 °C in a rotary shaker at 225 rpm. Starter cultures (25 mL) were grown overnight following inoculation with single colonies. Ten milliliters of the starter culture was then used to inoculate a 500 mL culture. Cell cultures were induced with 1 mM IPTG after the OD_{600} had reached 1.0 and incubated for an additional 4 h. The cells were pelleted at 5000*g* for 10 min at 4 °C and stored at −20 °C.

Protein Purification. Cell pellets were resuspended in 10 mL of lysis buffer [20 mM Tris, 1 mM EDTA, 1 g/L lysozyme, and 5 units benzonase nuclease (pH 7.5)] to which was added 250 μL of protease inhibitor cocktail per gram of pellet. The protease inhibitor cocktail contained 23 mM AEBSF, 2 mM bestatin, 0.3 mM pepstatin A2, and 0.3 mM E-64). The resuspended pellet was incubated at room temperature for 10 min with gentle shaking. Cellular debris was removed by centrifugation (15000*g* for 10 min at 4 °C). Protein purification chromatography steps were performed using a fast protein liquid chromatography (FPLC) system (ÄKTAPrime plus, GE Healthcare, Piscataway, NJ) at 4 °C using 214 nm detection. While both proteins were co-expressed in *E. coli* and share similar molecular masses, ACTR and CBP have drastically different theoretical pI values of 4.2 and 11.1, respectively.[36] Because of this, we chose ion exchange to isolate the two proteins. ACTR was purified using a buffer exchange step followed by anion exchange and gel filtration. The lysis buffer was exchanged for anion exchange buffer [50 mM piperazine (pH 9.0)] using a desalting column (HiPrep 26/10 Desalting, GE Healthcare). Collected protein fractions containing ACTR were identified by SDS−PAGE, pooled, and passed through an anion exchange column (HiTrap Q XL, GE Healthcare) in 50 mM piperazine using a 0 to 1 M NaCl gradient over 70 min at a rate of 1 mL/min. Fractions containing ACTR were identified by SDS−PAGE, pooled, then loaded onto a gel filtration column (HiPrep 16/60 Sephacryl S-100 HR, GE Healthcare), and eluted with 10 mM sodium phosphate and 50 mM NaCl buffer (pH 6.9). The ACTR stock concentration was 14 μM using a BCA assay[37] standardized with BSA (Thermo Fisher Scientific).

To purify CBP, we used a buffer exchange step followed by cation exchange and a second buffer exchange step. The clarified lysate was passed through a desalting column (HiPrep 26/10 Desalting, GE Healthcare) with 50 mM boric acid (pH 9.0). The buffer also contained 3 mM dithiothreitol (DTT) to prevent methionine oxidation. Collected protein fractions containing CBP were identified by SDS−PAGE and pooled. CBP was purified by cation exchange (HiTrap SP FF, GE Healthcare) using a 0 to 1 M NaCl gradient over 70 min in 50 mM boric acid and 3 mM DTT (pH 9.0) at a rate of 1 mL/min. Fractions containing CBP were identified by SDS−PAGE, pooled, then loaded onto the desalting column, and eluted into 10 mM phosphate, 50 mM NaCl, and 3 mM DTT buffer (pH 6.9). The CBP stock concentration was 17 μM using a BCA assay[37] standardized against BSA. DTT was removed by acetone precipitation and reconstitution in DTT-free buffer prior to the protein assay. Both ACTR and CBP protein identities were confirmed by mass spectrometry (results not shown). Protein stocks were split into aliquots, frozen with liquid nitrogen, and stored at −74 °C.

H/D Exchange Labeling. On the basis of the reported dissociation constant of 34 nM for the ACTR−CBP complex,[15] a 5-fold molar excess of CBP will bind more than 90% of ACTR, and vice versa under labeling conditions. Four sample pools were prepared to represent both ACTR and CBP in free and complex states. A 1:4.9 ACTR:CBP molar ratio was prepared by mixing 19 μL of ACTR stock with 81 μL of CBP

stock (complex). Under labeling conditions [1:20 dilution (see below)], 94% of ACTR is bound. Similarly, a 1:4.7 CBP:ACTR molar ratio was prepared by mixing 15 μL of CBP stock with 85 μL of ACTR stock (complex), yielding 93% bound CBP under labeling conditions. For the individual free proteins, an equal volume of phosphate buffer was substituted for the binding partner. All pools were incubated at room temperature for 1 h prior to deuterium labeling.

Samples were labeled by rapid dilution of 5 μL of a sample pool with 100 μL of 10 mM phosphate and 50 mM NaCl in D_2O (pD 6.9). After labeling intervals ranging between 5 s and 12 h, the labeling reaction was quenched with 17 μL of 0.1 M HCl to decrease the pH to 2.6. Undeuterated controls were prepared for each sample pool by mixing 5 μL of a sample with 100 μL of phosphate buffer in H_2O (pH 6.9) and 17 μL of 0.1 M HCl. Totally deuterated controls were prepared for each sample via dilution of 5 μL with 100 μL of phosphate buffer in D_2O (pH 6.9), followed by quenching after 24 h with 17 μL of 0.1 M HCl. After the reactions had been quenched, all samples were immediately flash-frozen with liquid nitrogen and stored at −74 °C. Individual samples were thawed by hand in approximately 2 min just prior to analysis.

Chromatography. An Agilent Technologies 1200 series isocratic pump and a 12-port injector valve (Valco Instruments Co. Inc.) were used to inject the loaded sample through a 50 mm × 2.1 mm immobilized pepsin column prepared in house as described previously[38] at a flow rate of 0.2 mL/min for 0.1% formic acid in water onto a self-packed C_{12} trap (10 mm × 1 mm) (Jupiter, Phenomenex, Torrence, CA) for 2.5 min to desalt and concentrate the samples. An Agilent Technologies 1200 series binary pump was used to conduct a high-performance liquid chromatography separation of peptic fragments. Solvent A was 0.1% formic acid in water, and solvent B was a 90% acetonitrile/10% water/0.1% formic acid mixture. Peptic peptides were separated on a C_{12} column (50 mm × 1 mm) (Jupiter Proteo, Phenomenex) using a water/acetonitrile gradient (10 to 35% B over 5 min at a rate of 50 μL/min). A thermoelectrically cooled system, constructed in house, kept the loop, valve, columns, and solvent lines at 0 °C.[39]

MS Analysis. Following separation, peptides were eluted into the electrospray ionization source of a time-of-flight mass spectrometer (model 6220, Agilent Technologies, Santa Clara, CA) operating in positive ion mode. Nitrogen at 325 °C and a flow rate of 10 L/min was used as the drying gas, with a nebulizer pressure of 30 psi. Fragmentor, skimmer, and capillary voltages were 150, 50, and 4000 V, respectively. Peptic peptides of undeuterated ACTR and CBP were identified by matching accurate mass measurements with a nonspecific protease digest in the MassHunter Qualitative Analysis with BioConfirm version B.03.01 (Agilent Technologies). To resolve ambiguous near-isobaric peptide assignments (±20 ppm), collision-induced dissociation (CID) product ion spectra were obtained by cycling the fragmentor voltage every 0.5 s among 150, 200, and 250 V. Observed fragment ion peaks were matched against b/y ion fragmentation predictions (Protein Prospector, MS-Product, http://prospector.ucsf.edu). The final list of identified peptides can be found in Table S1 of the Supporting Information. Using the expected retention times and molecular feature extraction in Qualitative Analysis with BioConfirm, mass spectra were extracted for each deuterated peptide sample. (The spectra can be found in Figure S1 of the Supporting Information.) HX-Express[40] was used to determine the average mass of each peptide using the portion of the isotopic distribution that was at least 20% of the base peak. Deuterium uptake for each peptide at each time point was calculated as the mass difference between the average peptide mass and the average mass of the undeuterated control. Our deuterium uptake results are presented without back-exchange correction.[27]

Intrinsic Exchange Calculations. The progress of intrinsic amide H/D exchange for unstructured peptides was calculated according to eq 1

$$D(t) = \sum_{i=3}^{m} [1 - e^{-k_{int}^{(i)} t}] \quad (1)$$

where m is the number of residues and $k_{int}^{(i)}$ is the rate constant for exchange for residue i of the peptide.[41] Proline residues were assigned a rate constant of zero because proline has no amide hydrogen. Upon proteolysis, the $i = 1$ amide hydrogen becomes a primary amine and hence back-exchanges rapidly during the LC step. Back-exchange at $i = 2$ is also generally quite rapid.[41,42] Thus, index i begins at 3, because there will be no deuterium remaining at $i \leq 2$. The calculations were implemented using an Excel spreadsheet (Microsoft, Redmond, WA) adapted from a spreadsheet available on W. Englander's website (http://hx2.med.upenn.edu). Our adapted version is available upon request. The intrinsic exchange calculations were normalized to the maximum observed deuterium uptake.

Kinetic Analysis. In this work, we have quantified the kinetics of H/D exchange using the method described by Englander and co-workers[43] in which the deuterium uptake has been fit to either a single- or double-stretched exponential function[43,44]:

$$D(t) = N[1 - e^{-(\langle k \rangle t)^{\beta}}]$$
$$D(t) = N_1[1 - e^{-(\langle k_1 \rangle t)^{\beta}}] + N_2[1 - e^{-(\langle k_2 \rangle t)^{\beta}}] \quad (2)$$

where $D(t)$ is the extent of deuteration as a function of D_2O exposure time t, N is the number of exchangeable amides, $\langle k \rangle$ represents the segment-averaged rate constant for exchange (for either intrinsic exchange, $\langle k_{int} \rangle$, or observed exchange, $\langle k_{HX} \rangle$), and β is an exponential stretching factor that accounts for the distribution in the intrinsic rates of H/D exchange of the individual amides. β was determined using a fit to the intrinsic exchange calculation (see eq 1). The fit to intrinsic exchange also yields the segment-averaged rate constant for intrinsic exchange, $\langle k_{int} \rangle$. The use of the stretched exponential function requires fewer adjustable parameters than the multiexponential[45,46] fits commonly used to describe H/D exchange kinetics, and thus, the nonlinear least-squares fit is more robust. In either case, because the resulting rate constants are segment-averaged, they are best considered "phenomenological"[47] rate constants. The ratio of the intrinsic exchange rate constant, $\langle k_{int} \rangle$, to the measured rate constant, $\langle k_{HX} \rangle$, can be used to estimate a segment-averaged protection factor, $\langle PF \rangle$, a measure of the slowing of exchange induced by the structure of the protein:

$$\langle PF \rangle = \frac{\langle k_{int} \rangle}{\langle k_{HX} \rangle} \quad (3)$$

An average protection factor of unity indicates a segment that is completely unstructured; i.e., the segment exchanges at its intrinsic rate. A protection factor greater than 1 indicates the region is protected from H/D exchange. Because the measured

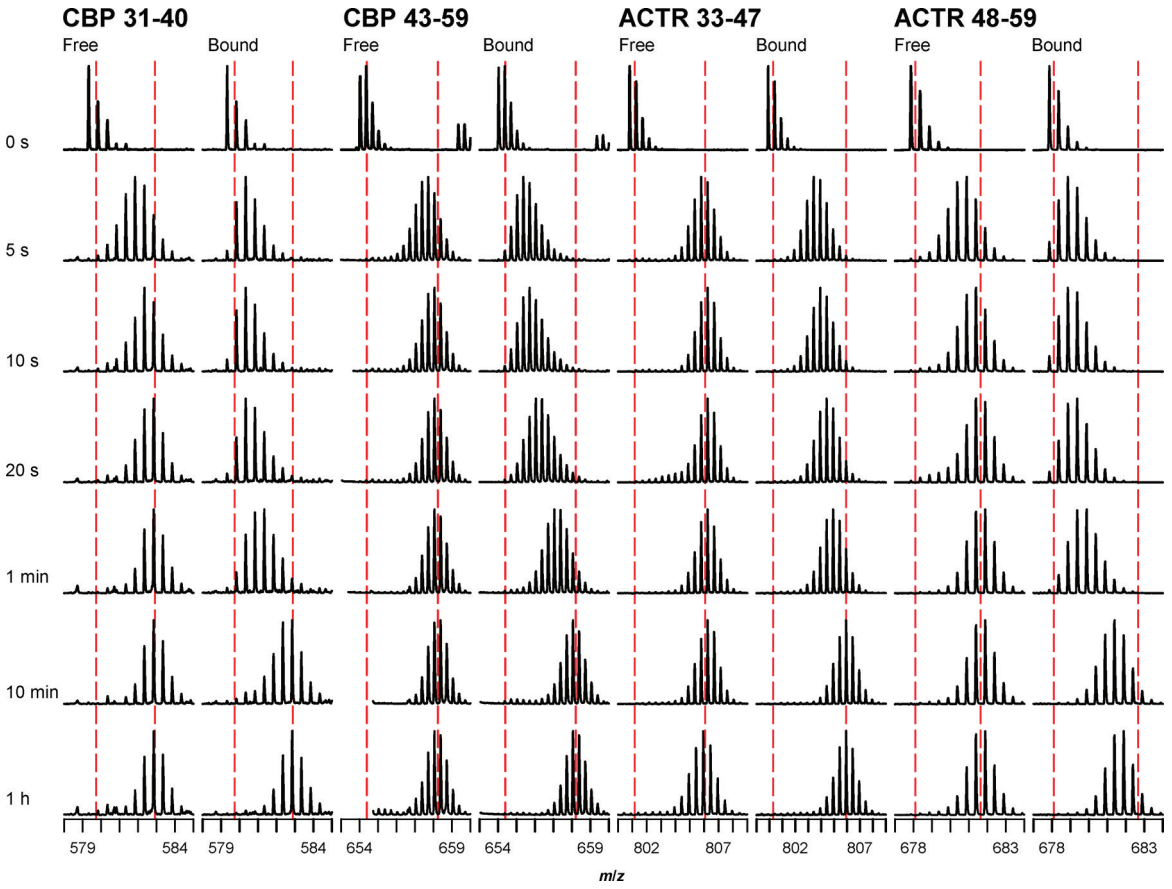

Figure 1. Mass spectra showing deuterium uptake in several distinctive regions of CBP and ACTR in both the free and bound states for selected D_2O exposure times. The vertical dashed lines denote the undeuterated (0 s) and fully deuterated (12 h) limits. The mass spectra show a steady progression of deuterium uptake with no evidence of bimodal isotope profiles.

H/D exchange is segment-averaged, these protection factors should not be interpreted thermodynamically as can be done for measurements obtained from single-residue resolution measurements.[26]

RESULTS

We initiated amide H/D exchange by rapidly diluting the individual proteins or the complex with a 19-fold excess of deuterated buffer. After intervals ranging from 5 s to 12 h, the exchange reaction was quenched by acidification. Under quench conditions, labile D is rapidly back-exchanged to H, but amide D back-exchanges much more slowly. To localize the exchange measurements to short linear segments of the proteins, the quenched samples were digested with pepsin, and then deuterium uptake as a function of D_2O exposure time was quantified via mass spectrometry. To compare the free and bound states of the proteins, H/D exchange was conducted for each protein separately and for each protein in the presence of a 5-fold molar excess of its binding partner (i.e., 1:5 CPB:ACTR and 5:1 CBP:ACTR).

Representative mass spectra from two segments of CBP (residues 31−40 and 43−59) and two segments of ACTR (residues 33−47 and 48−59) in both the free and bound states are shown in Figure 1. (See Figure S1 of the Supporting Information for a complete set of spectra for all segments.) The vertical dashed lines denote the average m/z values of the undeuterated and maximally deuterated forms. In the free state of CBP, both segments reach complete deuteration in less than 1 min. Upon formation of the CBP−ACTR complex, exchange in both CBP segments is slowed so that complete deuteration requires approximately 10 min. The 33−47 segment of ACTR exchanges much more quickly, becoming fully deuterated in less than 10 s, while the 48−59 segment is more protected and is not fully deuterated until exchange has occurred for 1 min. In the complex, both ACTR segments exchange more slowly, becoming fully deuterated in approximately 10 min. In all of the spectra shown in Figure 1, there is a steady progression of the isotopic envelopes across the mass range for both free and bound states. In particular, there is no evidence of a bimodal isotopic distribution, often taken to indicate H/D exchange by local or global unfolding through an EX1 mechanism.[22,48−50] There is also no evidence of bimodal isotopic distributions in any of the other peptides in either the free or bound states (see Figure S1 of the Supporting Information).

We quantified deuterium uptake by measuring the increase in the average mass of each segment. The mass increases for the segments shown in Figure 1, plotted as a function of time, are shown in Figure 2. Similar plots for all segments are provided in Figure S2 of the Supporting Information. For ease of viewing, the results are plotted in Figure 2 on both a logarithmic scale and a linear scale for the early exchange times. The maximum number of exchangeable amides is indicated by the limit of the vertical axis, and the horizontal dashed lines on the plots represent the maximum observed exchange, measured after samples had been exposed to D_2O for 12 h. Also plotted in Figure 2 is the intrinsic exchange for each segment calculated

dx.doi.org/10.1021/bi200875p | Biochemistry 2011, 50, 8722−8732

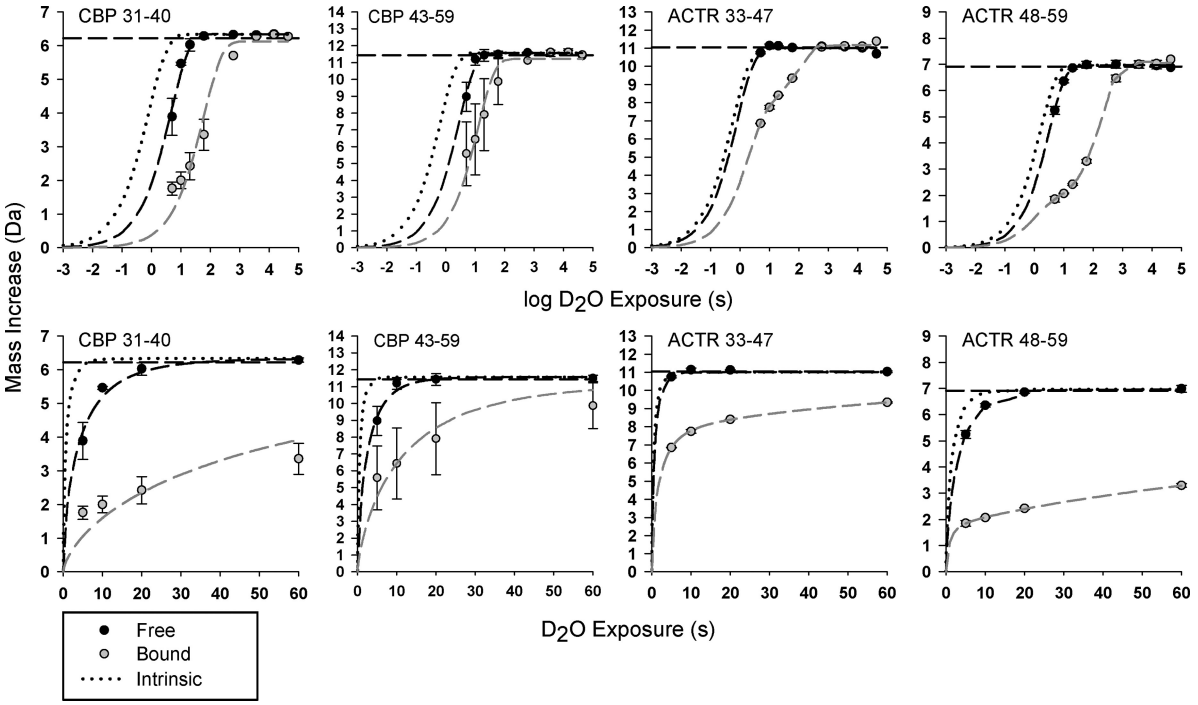

Figure 2. Deuterium uptake curves for the distinctive regions of CBP and ACTR shown in Figure 1. The top row of plots shows the full time course on a logarithmic scale, while the bottom row of plots shows the early time points on a linear scale. The dotted curves represent the calculated intrinsic rate of exchange calculated using eq 1. Deuterium uptake data are shown with data points, with black points representing uptake by the free proteins and gray points representing uptake by the proteins in the complex. Data points represent the average values obtained from two trials with error bars extended to the specific data points from each trial. Stretched exponential (or biexponential for ACTR peptides 33−42, 33−47, 36−47, and 48−59 in the complex state) curves overlay each set of data, with black broken curves and gray broken curves representing the free and protein complex states, respectively. For reference, the maximum deuterium uptake, measured after exchange for 24 h, is shown as a horizontal dashed line with the exception of the ACTR 60−71 segment, which did not produce a detectable spectral intensity. The maximum number of exchangeable amides ($n_{residues} - n_{proline} - 2$) is indicated by the limit of the vertical axis of the plot.

using eq 1. In the free state, both CBP 31−40 and CBP 43−59 segments are protected from exchange, as indicated by exchange slower than that predicted using the intrinsic calculation. In the free state, the ACTR 33−47 segment exchanges at the intrinsic rate, but the ACTR 48−59 segment is slightly protected from exchange. In the complex, all four segments become substantially more protected from exchange.

To quantify the extent of protection, we derived segment-averaged protection factors, ⟨PF⟩, by fitting the kinetic data to stretched exponential or biexponential functions (see eq 2).[43] The results of the kinetic analysis are listed in Table 1 and mapped onto the sequences of the proteins in Figure 3. For free ACTR, all segments exchange at or near the rate predicted for intrinsic exchange (Figure 2) with protection factors ranging from 1.0 to 2.4 (Table 1 and Figure 3). In the deuterium uptake plots, however, there is a clear distinction between segments that exchange at the calculated intrinsic rate and those that exchange more slowly. Deuterium uptake plots for segments 1−12, 33−42, 33−47, 36−47, and 60−71 capture only the plateau of H/D exchange (see Figure 2 and Figure S2 of the Supporting Information). In these segments, the observed H/D exchange is consistent with the intrinsic exchange calculation. In contrast, for the 13−22, 29−35, and 48−59 segments, our measurements at the 5 and 10 s points of D_2O exposure capture the knee of the H/D exchange curve and show clearly that these segments exchange more slowly than predicted by intrinsic exchange. Unlike ACTR, all segments in free CBP exchange more slowly than predicted by the intrinsic exchange calculation. Notably, all CBP segments follow similar H/D exchange kinetics, leading to a narrow range in the protection factors between 4.1 and 5.7 (see Table 1 and Figure 3). Hence, there is very little contrast between segments that span the helical core and segments that span the tails.

In the complex, there are substantial changes in protection in many but not all ACTR segments. Binding to CBP has no effect on exchange in the N- and C-terminal regions of ACTR (1−22 and 60−71). These regions exchange at the intrinsic rate, indicating that they remain unprotected. In the middle regions of ACTR (29−59), however, there is substantial slowing of H/D exchange. Several segments, for example, ACTR 48−59, show clear biexponential H/D exchange kinetics (see Figure 2). In the middle regions of ACTR, segment-averaged protection factors are as high as 180. The bimodal exchange kinetics allowed us to subdivide several of the segments,[45] wherein one part exchanges rapidly while other regions are more protected from exchange. We have estimated the number of amides involved in the biexponential fits as

$$\text{no. of amides with } \langle PF \rangle_{1,2} = \left(\frac{N_{1,2}}{N_1 + N_2} \right) N_{max} \quad (4)$$

where N_{max} is the maximum number of detectable amide exchanges. This essentially represents a back-exchange correction[27] for the protection factors. By this means, we have been able to differentiate regions with high and low protection factors within a single peptide segment. For example, the 33−42 region of ACTR in the complex encompasses both highly protected (⟨PF_2⟩ = 180; four

dx.doi.org/10.1021/bi200875p | Biochemistry 2011, 50, 8722−8732

Table 1. H/D Exchange Kinetic Data for Free and Bound CBP and ACTR

protein	segment	residues	intrinsic		free			complex							
			β	k_{int} (s^{-1})	N	$k_{HX,free}$ (s^{-1})	⟨PF⟩	N_1	N_2	k_{HX1} (s^{-1})	k_{HX2} (s^{-1})	⟨PF_1⟩	⟨PF_2⟩	⟨PF_1/PF_{free}⟩	⟨PF_2/PF_{free}⟩
ACTR	1−12	1018−1029	0.60	1.8	8.3	1.8	1.0	8.0		3.0		0.60		0.60	
ACTR	13−22	1030−1039	0.61	1.1	5.0	0.44	2.4	5.1		0.54		1.9		0.80	
ACTR	29−35	1046−1052	0.90	0.61	4.4	0.34	1.8	4.5		0.023		27		15	
ACTR	33−42	1050−1059	0.66	1.9	7.0	1.2	1.6	3.2	3.7	0.43	0.010	4.4	180	2.7	110
ACTR	33−47	1050−1064	0.72	1.7	11	1.3	1.4	7.3	3.9	0.56	0.011	3.1	150	2.3	110
ACTR	36−47	1053−1064	0.73	1.5	7.9	0.93	1.7	5.4	2.6	0.66	0.012	2.3	130	1.4	79
ACTR	48−59	1065−1076	0.77	0.63	7.0	0.31	2.0	1.6	5.5	1.1	0.0046	0.59	140	0.29	67
ACTR	60−71	1077−1088	0.57	1.0	7.4	0.67	1.6	7.7		0.59		1.8		1.1	
CBP	1−10	2059−2068	0.75	2.0	6.5	0.50	4.1	6.4		0.50		4.0		0.99	
CBP	1−14	2059−2072	0.70	1.3	9.3	0.30	4.2	8.9		0.11		12		2.7	
CBP	17−30	2075−2088	0.74	2.1	9.1	0.37	5.7	8.8		0.044		48		8.4	
CBP	30−38	2088−2096	0.64	1.3	5.7	0.24	5.4	5.5		0.022		59		11	
CBP	31−40	2089−2098	0.68	1.3	6.3	0.22	5.7	6.1		0.017		73		13	
CBP	40−43	2098−2101	0.97	1.4	2.1	0.28	5.0	2.0		0.017		84		17	
CBP	43−59	2101−2117	0.75	1.6	12	0.37	4.3	11		0.081		20		4.6	

residues) and weakly protected (⟨PF_1⟩ = 4.4; four residues) subsegments. This segment spans four residues of helix 1 and four residues of the linker between helix 1 and helix 2. Although the resolution of H/D-MS data does not define the exact locations of the two amide populations, we have presented the data in Figure 3 aligned with the known secondary structure of ACTR in the complex. Several other segments of ACTR spanning the helix 1 to helix 2 region (33−42, 33−47, and 36−47) also exhibit biexponential kinetics. The 62−71 segment spans both helix 3 and the unstructured C-terminal tail of ACTR, but there is no increase in protection in this region of ACTR in the complex.

The H/D exchange kinetics for CBP also change significantly upon complex formation. There are substantial increases in protection all along the length of CBP (Table 1 and Figure 3). The largest increases in protection are in the Cα2 and Cα3 regions and in the linker connecting the two (residues 30−38, 31−40, and 40−43). Here, segment-averaged protection factors increase from ∼6 to 59−84. Protection also increases in the segments covering the N-terminal half of Cα1 and the C-terminal half of Cα3; however, the increases are not as large because these segments also cover the N- and C-terminal tails, respectively.

Figure 4 summarizes the effects of coupled binding and folding on the exchange kinetics. The figure shows the magnitude of the changes in segment-averaged protection, ⟨$PF_{complex}$⟩/⟨PF_{free}⟩, that accompany complex formation. The observed increases in the protection factor in ACTR in the complex range from ∼1-fold in the terminal regions to ∼100-fold in helix 2 of ACTR. The C-terminal half of helix Aα1 and all of helix Aα2 become highly protected in the complex (see panels a and b of Figure 4), but the linker between Aα1 and Aα2 remains unprotected from H/D exchange. The largest increase in the protection factor was in the N-terminal half of Aα3 (residues 55−59), while the 60−71 segment that covers the last two residues of Aα3 (62 and 63) has no increase in protection.

Compared with ACTR, there are only modest increases in the protection factor in CBP (9−17-fold) in the complex (Figure 4c,d). This effect can be attributed to greater protection in free CBP that increases the denominator in the protection ratio. Our H/D exchange measurements show that the C-terminal half of Cα2 and the N-terminal half of Cα3 (residues 30−43) become the most highly protected regions of bound CBP. There are only small increases in the protection factor in bound CBP in the segments that span the N-terminus of Cα1 and the C-terminus of Cα3 (residues 1−14 and 43−59, respectively). The protection factor in the 17−30 segment of bound CBP is greater than in the tail regions, but less than in the central core of CBP. Because the 17−30 segment spans the long linker between Cα1 and Cα2 and the flexible polyQ region, a limited increase in protection here is consistent with flexibility in this region of bound CBP.[51]

DISCUSSION

Model IDPs. Our objective in this work was to explore the capabilities and limitations of equilibrium H/D exchange to characterize intrinsically disordered proteins and reveal the details of their unstructured-to-structured transitions. The intrinsically disordered interaction domains of CBP and ACTR[51] serve as useful model systems because both the free domains and their cofolded complex have been well-characterized.[15,51−54] To place our results within the context

dx.doi.org/10.1021/bi200875p | Biochemistry 2011, 50, 8722−8732

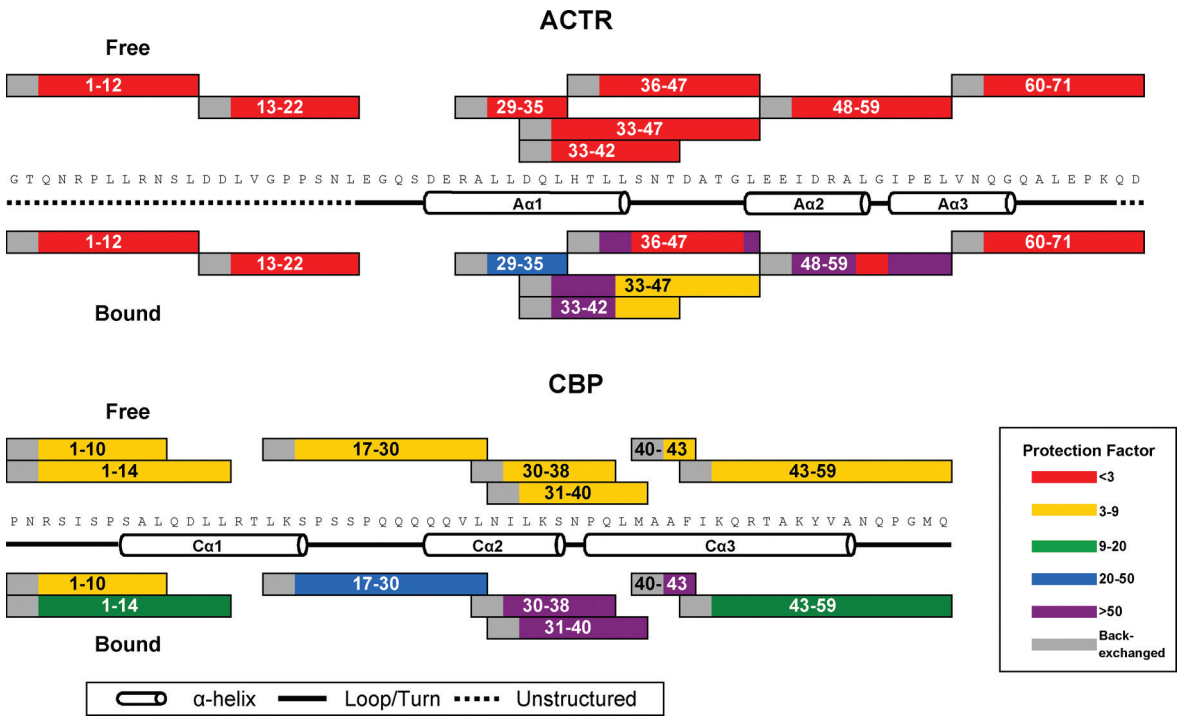

Figure 3. Protection factors mapped onto the sequences of ACTR and CBP for each peptide for both free and bound forms. The assigned secondary structural elements from the CBP−/ACTR complex[15] are also indicated. The first two residues of each peptide are colored gray to indicate that rapid back-exchange of the deuterium label at these two positions leads to no measurable deuterium uptake.

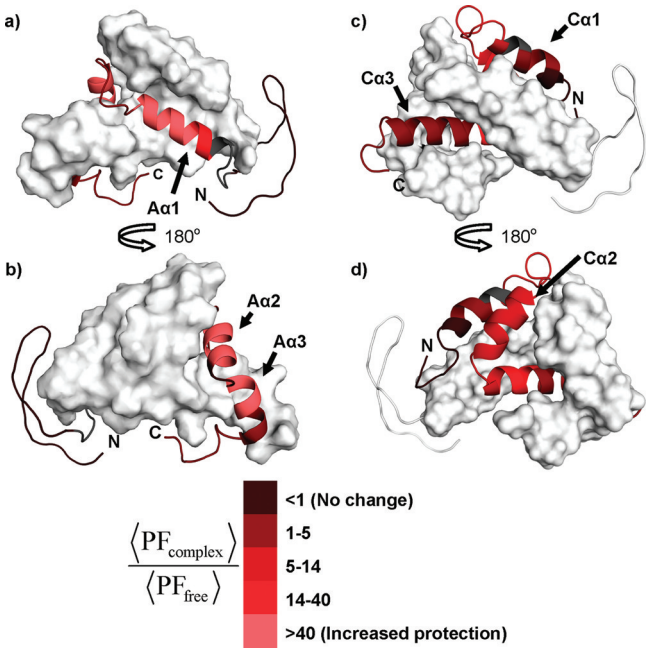

Figure 4. Structure of the ACTR−CBP complex (PDB entry 1KBH)[15] showing relative increases in the protection factor of (a and b) ACTR and (c and d) CBP that accompany complex formation. The cognate binding partner is shown in surface representation. In panels a and b, a modeled unstructured N-terminal region was appended to the NMR structure of ACTR. This figure was rendered using Pymol (version 0.99, DeLano Scientific, South San Francisco, CA).

of what is known about CBP and ACTR, we begin with a brief review.

On the basis of extensive NMR relaxation data and secondary chemical shifts, Ebert and co-workers[51] concluded that ACTR had the characteristics of an unstructured random coil. More recently, the conformation of free ACTR was interrogated using CD, small-angle X-ray scattering (SAXS), and multidimensional NMR.[54] In particular, secondary chemical shift measurements using reference shifts obtained from ACTR in urea indicated that there was a small percentage of α-helical propensity in the three regions of ACTR that form helices in the complex, particularly in helix 1.

On the basis of NMR, CD, and urea unfolding, CBP has been described as a molten globule, but its ensemble is sufficiently well-defined that structures have been determined.[53,55] NMR secondary chemical shift measurements show well-formed helical structure in free CBP.[51] The recent ensemble of structures[53] shows that CBP has a fairly well-defined hydrophobic core comprising all three helices that aligns well with the structure of CBP in the complex,[15] but the N- and C-terminal regions are less well-defined. CBP is only marginally stable and undergoes two-state unfolding with a ΔG_u of 6.1 ± 0.4 kJ/mol,[53] from which it follows that approximately 8% of the CBP population occupies conformers belonging to the unfolded subpopulation at 300 K. The absence of additional peaks in the NMR spectrum of free CBP led to the proposal that CBP interconverts between different conformers slightly faster than intermediate exchange (10^4 s^{-1}).[53]

CBP and ACTR form a tight 1:1 complex (K_d = 34 nM) with well-defined tertiary structure. The structure consists of a helical bundle in which a series of leucine side chains in helix 1 of ACTR lie in a hydrophobic groove between helices 1 and 3 of CBP (see Figure 4).[15] Secondary chemical shift measurements show dramatic increases in the levels of secondary structure across all of Aα1 and Aα2 but only a slight increase in the levels of secondary structure on the N-terminal side of helix Cα1 and the C-terminal end of helix Cα3.[51] Relaxation

dx.doi.org/10.1021/bi200875p | Biochemistry 2011, 50, 8722–8732

measurements show that both proteins become less dynamic in the complex.[51]

Limited, Uniform Protection Reveals Conformational Interconversion by Free CBP. Our results show that free CBP is slightly protected from exchange and that the exchange is nearly uniform in all segments (see Figure 3). The magnitude of the protection factors in CBP appears to be near the lower limit typically observed in the structured elements of molten globules. For example, in molten globular apomyoglobin, protection factors ranged from 5 to 200 in helical regions,[56] and in the β-sheet molten globular variant of bovine pancreatic trypsin inhibitor, protection factors ranging between 10 and 40 were found in the antiparallel β-sheet region.[57] More significantly, there is little differentiation in protection between segments in CBP. For example, the CBP 31−40 segment, spanning the most well-defined part of the CBP core, has a ⟨PF⟩ of 6, while the CBP 43−59 segment, spanning the loosely structured C-terminal half of helix 3 and the ill-defined C-terminal tail, has a ⟨PF⟩ of 4. Given the differences in these two regions, one would expect that the CBP 31−40 segment should be significantly more protected than the CBP 43−59 segment.

The apparent inconsistency between our measurements and the available data can be resolved if we interpret our data in terms of a two-process model of H/D exchange[58,59] as illustrated conceptually in Figure 5. In this figure, CBP is

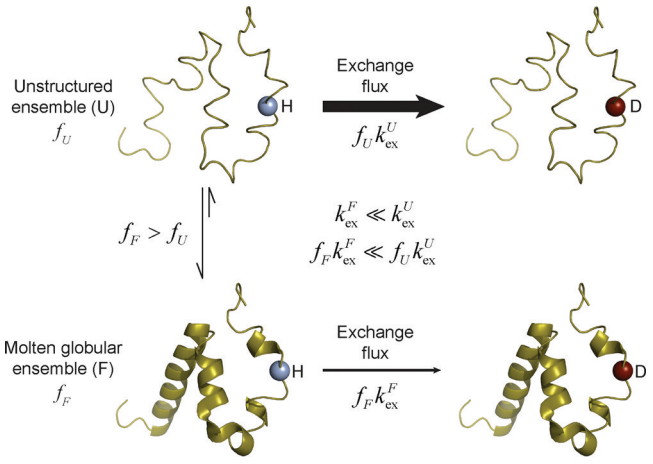

Figure 5. This conceptual representation of the H/D exchange flux model illustrates how limited, uniform protection observed for free CBP can be explained by interconversion between an ensemble of folded conformers and an ensemble of unstructured conformers. Because the unstructured conformers are much less protected from exchange, most of the total flux of exchange occurs through the unstructured ensemble, as depicted by the heavy arrow. See the text for additional details. The protein structures presented in this figure are conceptual models only and do not imply any structural details about the conformations. This figure was rendered with Pymol (version 0.99, DeLano Scientific) using the structure of CBP from the CBP−ACTR complex (PDB entry 1KBH)[15] as a starting point.

represented as an interconverting population of molecules that occupy both molten globular conformers and unstructured conformers. The H/D exchange flux[60,61] occurs through two separate channels: conformers of the molten globular ensemble and conformers of the unstructured ensemble. While the Boltzman weight of the molten globular conformers is much larger (f_F in Figure 5), these conformers are more protected from exchange (k_{ex}^F and k_{ex}^U). Conversely, CBP conformers occupying the unstructured ensemble have a much smaller Boltzmann weight (f_U in Figure 5) but are nearly or completely unprotected. Thus, the overall exchange flux is dominated by H/D exchange through unfolded conformers because of the rapid interconversion between the two populations.

The small, nearly uniform protection factors for free CBP shown in Figure 3 are consistent with a well-defined, protected molten globular ensemble of CBP conformers that rapidly interconvert with a population of unprotected conformers. Both the uniformity of protection and the small magnitude of the protection factors arise because the majority of H/D exchange occurs during intervals when CBP molecules occupy unprotected conformations. Because the accepted model of the molten globular state has well-defined secondary structure, but fluctuating tertiary structure, protection against exchange has often been taken as evidence of the existence of well-defined secondary structure. The preceding discussion offers an explanation for the limited, uniform protection that we find in molten globular CBP. Our results support the conclusion of Kjaergaard et al. that CBP occupies both a molten globular ensemble and an unstructured ensemble.[53] Our results also indicate that CBP lacks a consistently stable core in the unstructured ensemble. If such a core existed, then there would be more protection in the core region(s) than in regions outside of the core because the core regions would remain protected in all conformers. This result suggests that despite possessing well-defined conformers with a large Boltzmann weight, formation of complexes with CBP could involve coupled folding and binding as opposed to a strictly conformational selection-based mechanism.[62,63]

The absence of bimodal isotopic profiles in the mass spectra of the CBP segments indicates that CBP only transiently occupies unstructured conformations, supporting the rapid interconversion proposed by Kjaergaard et al.[53] If the lifetime of the unstructured, conformations was long relative to the length of intrinsic exchange, then a bimodal isotopic profile[24,48−50] would be evident in our spectra because an unstructured peptide segment would become fully deuterated during its time in an unprotected conformation. Because there is no evidence of such bimodal isotope profiles in any of the CBP peptides (see Figures 1 and Figure S1 of the Supporting Information), we conclude that the lifetime of the unstructured conformers must be on the scale of milliseconds or shorter (i.e., much less than k_{int}^{-1}, which is on the order of 1 s at pD 7[41]). The transient nature is consistent with the exchange constant ($k_F + k_U$) of 10^4 s^{-1} estimated by NMR.[53] This dynamic behavior is different than slow conformational interconversion detected in previous H/D-MS work with SH3 domains.[48,64,65]

Residual Structure in ACTR. While most segments in ACTR exchange at the intrinsic rate, H/D exchange is slower than predicted in the 29−35 and 48−59 segments, consistent with secondary chemical shift measurements that showed a slight helical propensity in these regions.[54] Like CBP, there is no indication of bimodal isotope profiles at the early exchange time points in these slightly protected segments (see Figure 1, ACTR 48−59, and Figure S1 of the Supporting Information, ACTR 29−35). From this, we conclude that these slightly protected regions interconvert with unprotected conformations on a time scale that is much faster than that of intrinsic exchange (0.1−1 s). Thus, fully unprotected conformers in the ACTR conformational ensemble exist. Equilibrium H/D exchange measured on the millisecond time scale using quench

flow[66,67] may yield additional insight into the nature of the transient helical structure in ACTR.

Formation of the ACTR−CBP Complex. Three factors can contribute to increased protection factors in the complex: stabilization of secondary structure, slowed dynamics, and interface protection. Competing against these protecting effects is the dynamic equilibrium between the complex and the less protected free proteins.[25] If the on rate for complex formation is slow on the H/D exchange time scale, then H/D exchange would involve two discrete populations, a minority of rapidly exchanging free protein (∼5%) and a majority (∼95%) of slowly exchanging protein in the complex. As was observed with the free proteins, the MS spectra show no evidence of bimodal isotopic distributions (see Figure 1 and Figure S1 of the Supporting Information). In particular, there is no evidence at early D_2O exposure times of fully deuterated peptides in the spectra from the complex. Such an exchange scenario is distinct from the biexponential kinetics used to fit the ACTR data. In the biexponential case, two subsets of amides in a segment exchange at different rates. In the case of fast- and slow-exchanging populations, all amides in a segment would exchange by both processes. Because of the absence of bimodal isotope profiles, we conclude that the complex forms and folds rapidly from the free proteins relative to the time scale of intrinsic exchange.

In cases of coupled binding and folding, where the free states are only weakly protected, there will not be large protection factors in the complex except at highly saturating ligand concentrations. The reason for this is that the observed exchange kinetics will be dictated by the brief intervals when the proteins are ligand-free and unprotected.[61] Despite the limitations, we can nevertheless derive valuable insight into coupled binding and folding in the CBP−ACTR complex on the basis of relative changes in protection. Our H/D-MS results show that the regions involved in binding and/or folding can be readily identified by increased protection factors in the complex. The largest increases in protection are found in the regions of ACTR that make hydrophobic side chain contacts with hydrophobic residues lining a groove in CBP. CBP, which is already more well-defined in the free state, shows much smaller increases in protection in the complex, but as with ACTR, the largest increases map to the core of the complex.

Application of H/D-MS to IDPs. In this work, we have evaluated the capabilities of H/D-MS to characterize the model IDPs CBP and ACTR and their synergistically folded complex. Our work shows that the picture of ACTR and CBP that emerges from our H/D exchange measurements is consistent with previous biophysical measurements. With ACTR, we have shown that analysis of segment-averaged H/D exchange kinetics can be used to identify residual structure in unstructured IDPs. With CBP, interconversion between structured and unstructured conformers was revealed by limited but nearly uniform protection. An important point that emerges from this work is that the seemingly rapid, uniform exchange, as we observed with CBP, could be easily misinterpreted as indicating an unstructured protein. In this regard, intrinsic exchange calculations serve as a useful upper bound for H/D exchange kinetics, clearly showing that exchange by CBP cannot simply be dismissed as rapid. In the case of ACTR, these calculations were again useful, this time highlighting the presence of residual structure.

H/D-MS promises to contribute to good progress in the difficult terrain of intrinsically disordered proteins. While peptide-level H/D exchange lacks the single-amide resolution afforded by NMR, mass spectrometry offers two distinct advantages. First, MS measurements require only picomole quantities of protein at micromolar concentrations. Given the difficulty that many laboratories have encountered in the expression and purification of recombinant IDPs, there may simply never be enough protein for NMR or other biophysical methods. The second advantage of mass spectrometry is that protein mass is nearly unlimited. Recent work with ∼150 kDa monoclonal antibodies[68] and viral assemblies[69] has clearly demonstrated the ability of H/D-MS to handle large proteins and protein complexes. In large proteins, identification of short unstructured molecular recognition features (MoRFs) that undergo coupled binding and folding[70] would be difficult with any other technique.

Our work also reveals an important need for better kinetic models to interpret segment-averaged H/D exchange kinetics. While the stretched exponential equation[43,44] does seem to empirically describe H/D exchange kinetics, the theoretical basis for its use and for the interpretation of the derived parameters is currently lacking. In the absence of a good model for justifying the use of the stretched exponential function, we believe derivation of thermodynamic values from segment-averaged protection should be approached with caution. There is clearly a need for an extension of the two-process model of H/D exchange to explicitly address both segment averaging and the departure of IDPs from exchange under the conventional kinetic limits. We speculate that such an extension might lend new insight into the analysis of the H/D exchange kinetics of IDPs.

■ ASSOCIATED CONTENT

Ⓢ Supporting Information

Table of the peptic peptide assignments (Table S1), mass spectra of all undeuterated and deuterated peptides (Figure S1), and deuterium uptake curves for all segments (Figure S2). This material is available free of charge via the Internet at http://pubs.acs.org.

■ AUTHOR INFORMATION

Corresponding Author

*Telephone: (785) 864-1377. Fax: (785) 864-5396. E-mail: dweis@ku.edu.

Funding

Financial support for this research from the University of Kansas is gratefully acknowledged.

■ ACKNOWLEDGMENTS

We thank Prof. Peter Wright (The Scripps Research Institute, La Jolla, CA) for the CBP−ACTR coexpression plasmid, Dr. Todd Williams (University of Kansas) for assistance with MS/MS identification of the peptic peptides, and Prof. Richard Schowen (University of Kansas) for helpful discussions.

■ ABBREVIATIONS

ACTR, activator of thyroid and retinoid receptors; AEBSF, 4-(2-aminoethyl)benzenesulfonyl fluoride hydrochloride; BCA, bicinchoninic acid; CBP, CREB binding protein; CID, collision-induced dissociation; CREB, cyclic adenosine monophosphate-responsive element-binding protein; DTT, D,L-dithiothreitol; EDTA, ethylenediaminetetraacetic acid; FPLC, fast protein liquid chromatography; H/D-MS, hydrogen/

deuterium exchange mass spectrometry; IDP, intrinsically disordered protein; IPTG, isopropyl β-D-1-thiogalactopyranoside; LC, liquid chromatography; MS, mass spectrometry; NMR, nuclear magnetic resonance spectroscopy; OD_{600}, optical density measured at 600 nm; SDS−PAGE, sodium dodecyl sulfate−polyacrylamide gel electrophoresis.

REFERENCES

(1) Sigler, P. B. (1988) Acid blobs and negative noodles. *Nature 333*, 210−212.

(2) Kriwacki, R. W., Hengst, L., Tennant, L., Reed, S. I., and Wright, P. E. (1996) Structural studies of p21Waf1/Cip1/Sdi1 in the free and Cdk2-bound state: Conformational disorder mediates binding diversity. *Proc. Natl. Acad. Sci. U.S.A. 93*, 11504−11509.

(3) Garner, E., Cannon, P., Romero, P., Obradovic, Z., and Dunker, A. K. (1998) Predicting disordered regions from amino acid sequence: Common themes despite differing structural characterization. *Genome Inf. Ser. 9*, 201−213.

(4) Wright, P. E., and Dyson, H. J. (1999) Intrinsically unstructured proteins: Re-assessing the protein structure-function paradigm. *J. Mol. Biol. 293*, 321−331.

(5) Uversky, V. N., Gillespie, J. R., and Fink, A. L. (2000) Why are "natively unfolded" proteins unstructured under physiologic conditions? *Proteins 41*, 415−427.

(6) Dunker, A. K., Brown, C. J., Lawson, J. D., Iakoucheva, L. M., and Obradovic, Z. (2002) Intrinsic disorder and protein function. *Biochemistry 41*, 6573−6582.

(7) Uversky, V. N. (2002) Natively unfolded proteins: A point where biology waits for physics. *Protein Sci. 11*, 739−756.

(8) Dyson, H. J., and Wright, P. E. (2005) Intrinsically unstructured proteins and their functions. *Nat. Rev. Mol. Cell Biol. 6*, 197−208.

(9) Tompa, P., Fuxreiter, M., Oldfield, C. J., Simon, I., Dunker, A. K., and Uversky, V. N. (2009) Close encounters of the third kind: Disordered domains and the interactions of proteins. *BioEssays 31*, 328−335.

(10) Gsponer, J., and Babu, M. M. (2009) The rules of disorder or why disorder rules. *Prog. Biophys. Mol. Biol. 99*, 94−103.

(11) Uversky, V. N., and Dunker, A. K. (2010) Understanding protein non-folding. *Biochim. Biophys. Acta 1804*, 1231−1264.

(12) He, B., Wang, K., Liu, Y., Xue, B., Uversky, V. N., and Dunker, A. K. (2009) Predicting intrinsic disorder in proteins: An overview. *Cell Res. 19*, 929−949.

(13) Gsponer, J., Futschik, M. E., Teichmann, S. A., and Babu, M. M. (2008) Tight regulation of unstructured proteins: From transcript synthesis to protein degradation. *Science 322*, 1365−1368.

(14) Xie, H., Vucetic, S., Iakoucheva, L. M., Oldfield, C. J., Dunker, A. K., Uversky, V. N., and Obradovic, Z. (2007) Functional anthology of intrinsic disorder. 1. Biological processes and functions of proteins with long disordered regions. *J. Proteome Res. 6*, 1882−1898.

(15) Demarest, S. J., Martinez-Yamout, M., Chung, J., Chen, H., Xu, W., Dyson, H. J., Evans, R. M., and Wright, P. E. (2002) Mutual synergistic folding in recruitment of CBP/p300 by p160 nuclear receptor coactivators. *Nature 415*, 549−553.

(16) Lacy, E. R., Filippov, I., Lewis, W. S., Otieno, S., Xiao, L., Weiss, S., Hengst, L., and Kriwacki, R. W. (2004) p27 binds cyclin-CDK complexes through a sequential mechanism involving binding-induced protein folding. *Nat. Struct. Mol. Biol. 11*, 358−364.

(17) Shoemaker, B. A., Portman, J. J., and Wolynes, P. G. (2000) Speeding molecular recognition by using the folding funnel: The fly-casting mechanism. *Proc. Natl. Acad. Sci. U.S.A. 97*, 8868−8873.

(18) Uversky, V. N., Oldfield, C. J., and Dunker, A. K. (2008) Intrinsically disordered proteins in human diseases: Introducing the D-2 concept. *Annu. Rev. Biophys. 37*, 215−246.

(19) Receveur-Bréchot, V., Bourhis, J.-M., Uversky, V. N., Canard, B., and Longhi, S. (2006) Assessing protein disorder and induced folding. *Proteins 62*, 24−45.

(20) Eliezer, D. (2009) Biophysical characterization of intrinsically disordered proteins. *Curr. Opin. Struct. Biol. 19*, 23−30.

(21) Wright, P. E., and Dyson, H. J. (2009) Linking folding and binding. *Curr. Opin. Struct. Biol. 19*, 31−38.

(22) Hvidt, A., and Nielsen, S. O. (1966) Hydrogen exchange in proteins. *Adv. Protein Chem. 21*, 287−385.

(23) Englander, S. W., and Kallenbach, N. R. (1984) Hydrogen exchange and structural dynamics of proteins and nucleic acids. *Q. Rev. Biophys. 16*, 521−655.

(24) Konermann, L., Tong, X., and Pan, Y. (2008) Protein structure and dynamics studied by mass spectrometry: H/D exchange, hydroxyl radical labeling, and related approaches. *J. Mass Spectrom. 43*, 1021−1036.

(25) Mayne, L., Paterson, Y., Cerasoli, D., and Englander, S. W. (1992) Effect of antibody binding on protein motions studied by hydrogen-exchange labeling and two-dimensional NMR. *Biochemistry 31*, 10678−10685.

(26) Bai, Y., Sosnick, T. R., Leland, M., and Englander, S. W. (1995) Protein folding intermediates: Native-state hydrogen exchange. *Science 269*, 192−197.

(27) Zhang, Z., and Smith, D. L. (1993) Determination of amide hydrogen exchange by mass spectrometry: A new tool for protein structure elucidation. *Protein Sci. 2*, 522−531.

(28) Pan, J., Han, J., Borchers, C. H., and Konermann, L. (2009) Hydrogen/deuterium exchange mass spectrometry with top-down electron capture dissociation for characterizing structural transitions of a 17 kDa protein. *J. Am. Chem. Soc. 131*, 12801−12808.

(29) Sharma, S., Zheng, H., Huang, Y. J., Ertekin, A., Hamuro, Y., Rossi, P., Tejero, R., Acton, T. B., Xiao, R., Jiang, M., Zhao, L., Ma, L.-C., Swapna, G. V. T., Aramini, J. M., and Montelione, G. T. (2009) Construct optimization for protein NMR structure analysis using amide hydrogen/deuterium exchange mass spectrometry. *Proteins 76*, 882−894.

(30) Pantazatos, D., Kim, J. S., Klock, H. E., Stevens, R. C., Wilson, I. A., Lesley, S. A., and Woods, V. L. (2004) Rapid refinement of crystallographic protein construct definition employing enhanced hydrogen/deuterium exchange MS. *Proc. Natl. Acad. Sci. U.S.A. 101*, 751−756.

(31) Mazon, H., Marcillat, O., Forest, E., and Vial, C. (2005) Denaturant sensitive regions in creatine kinase identified by hydrogen/deuterium exchange. *Rapid Commun. Mass Spectrom. 19*, 1461−1468.

(32) Raza, A. S., Dharmasiri, K., and Smith, D. L. (2000) Identification of non-covalent structure in apocytochrome c by hydrogen exchange and mass spectrometry. *J. Mass Spectrom. 35*, 612−617.

(33) Mitchell, J. L., Trible, R. P., Emert-Sedlak, L. A., Weis, D. D., Lerner, E. C., Applen, J. J., Sefton, B. M., Smithgall, T. E., and Engen, J. R. (2007) Functional characterization and conformational analysis of the *Herpesvirus saimiri* Tip-C484 protein. *J. Mol. Biol. 366*, 1282−1293.

(34) Hansen, J. C., Wexler, B. B., Rogers, D. J., Hite, K. C., Panchenko, T., Ajith, S., and Black, B. E. (2011) DNA binding restricts the intrinsic conformational flexibility of MeCP2. *J. Biol. Chem. 286*, 18938−18948.

(35) Croy, C. H., Bergqvist, S., Huxford, T., Ghosh, G., and Komives, E. A. (2004) Biophysical characterization of the free IκBα ankyrin repeat domain in solution. *Protein Sci. 13*, 1767−1777.

(36) Gasteiger, E., Gattiker, A., Hoogland, C., Ivanyi, I., Appel, R. D., and Bairoch, A. (2003) ExPASy: The proteomics server for in-depth protein knowledge and analysis. *Nucleic Acids Res. 31*, 3784−3788.

(37) Smith, P. K., Krohn, R. I., Hermanson, G. T., Mallia, A. K., Gartner, F. H., Provenzano, M. D., Fujimoto, E. K., Goeke, N. M., Olson, B. J., and Klenk, D. C. (1985) Measurement of protein using bicinchoninic acid. *Anal. Biochem. 150*, 76−85.

(38) Wang, L., Pan, H., and Smith, D. L. (2002) Hydrogen exchange-mass spectrometry: Optimization of digestion conditions. *Mol. Cell. Proteomics 1*, 132−138.

(39) Keppel, T. R., Jacques, M. E., Young, R. W., Ratzlaff, K. L., and Weis, D. D. (2011) An efficient and inexpensive refrigerated LC system for H/D exchange mass spectrometry. *J. Am. Soc. Mass Spectrom. 22*, 1472−1476.

(40) Weis, D. D., Engen, J. R., and Kass, I. J. (2006) Semi-automated data processing of hydrogen exchange mass spectra using HX-Express. *J. Am. Soc. Mass Spectrom. 17*, 1700−1703.
(41) Bai, Y., Milne, J. S., Mayne, L., and Englander, S. W. (1993) Primary structure effects on peptide group hydrogen exchange. *Proteins 17*, 75−86.
(42) Connelly, G. P., Bai, Y., Jeng, M.-F., and Englander, S. W. (1993) Isotope effects in peptide group hydrogen exchange. *Proteins 17*, 87−92.
(43) Chetty, P. S., Mayne, L., Lund-Katz, S., Stranz, D., Englander, S. W., and Phillips, M. C. (2009) Helical structure and stability in human apolipoprotein A-I by hydrogen exchange and mass spectrometry. *Proc. Natl. Acad. Sci. U.S.A. 106*, 19005−19010.
(44) Dewey, T. G. (1994) Fractal analysis of proton exchange kinetics in lysozyme. *Proc. Natl. Acad. Sci. U.S.A. 91*, 12101−12104.
(45) Resing, K. A., Hoofnagle, A. N., and Ahn, N. G. (1999) Modeling deuterium exchange behavior of ERK2 using pepsin mapping to probe secondary structure. *J. Am. Soc. Mass Spectrom. 10*, 685−702.
(46) Codreanu, S. G., Ladner, J. E., Xiao, G., Stourman, N. V., Hachey, D. L., Gilliland, G. L., and Armstrong, R. N. (2002) Local protein dynamics and catalysis: Detection of segmental motion associated with rate-limiting product release by a glutathione transferase. *Biochemistry 41*, 15161−15172.
(47) Konermann, L., Pan, J., and Liu, Y.-H. (2011) Hydrogen exchange mass spectrometry for studying protein structure and dynamics. *Chem. Soc. Rev. 40*, 1224−1234.
(48) Engen, J. R., Smithgall, T. E., Gmeiner, W. H., and Smith, D. L. (1997) Identification and localization of slow, natural, cooperative unfolding in the hematopoietic cell kinase SH3 domain by amide hydrogen exchange and mass spectrometry. *Biochemistry 36*, 14384−14391.
(49) Xiao, H., Hoerner, J. K., Eyles, S. J., Dobo, A., Voigtman, E., Mel'čuk, A. I., and Kaltashov, I. A. (2005) Mapping protein energy landscapes with amide hydrogen exchange and mass spectrometry: I. A generalized model for a two-state protein and comparison with experiment. *Protein Sci. 14*, 543−557.
(50) Weis, D. D., Wales, T. E., Engen, J. R., Hotchko, M., and Ten Eyck, L. F. (2006) Identification and characterization of EX1 kinetics in H/D exchange mass spectrometry by peak width analysis. *J. Am. Soc. Mass Spectrom. 17*, 1498−1509.
(51) Ebert, M.-O., Bae, S.-H., Dyson, H. J., and Wright, P. E. (2008) NMR relaxation study of the complex formed between CBP and the activation domain of the nuclear hormone receptor coactivator ACTR. *Biochemistry 47*, 1299−1308.
(52) Demarest, S. J., Deechongkit, S., Dyson, H. J., Evans, R. M., and Wright, P. E. (2004) Packing, specificity, and mutability at the binding interface between the p160 coactivator and CREB-binding protein. *Protein Sci. 13*, 203−210.
(53) Kjaergaard, M., Teilum, K., and Poulsen, F. M. (2010) Conformational selection in the molten globule state of the nuclear coactivator binding domain of CBP. *Proc. Natl. Acad. Sci. U.S.A. 107*, 12535−12540.
(54) Kjaergaard, M., Nørholm, A., Hendus−Altenburger, R., Pedersen, S. F., Poulsen, F. M., and Kragelund, B. B. (2010) Temperature-dependent structural changes in intrinsically disordered proteins: Formation of α-helices or loss of polyproline II? *Protein Sci. 19*, 1555−1564.
(55) Lin, C. H., Hare, B. J., Wagner, G., Harrison, S. C., Maniatis, T., and Fraenkel, E. (2001) A small domain of CBP/p300 binds diverse proteins: solution structure and functional studies. *Mol. Cell 8*, 581−590.
(56) Hughson, F.M., Wright, P. E., and Baldwin, R. L. (1990) Structural characterization of a partly folded apomyoglobin intermediate. *Science 249*, 1544−1548.
(57) Barbar, E., Barany, G., and Woodward, C. (1995) Dynamic structure of a highly ordered β-sheet molten globule: Multiple conformations with a stable core. *Biochemistry 34*, 11423−11434.
(58) Woodward, C. K., and Hilton, B. D. (1980) Hydrogen isotope exchange kinetics of single protons in bovine pancreatic trypsin inhibitor. *Biophys. J. 32*, 561−575.
(59) Qian, H., and Chan, S. I. (1999) Hydrogen exchange kinetics of proteins in denaturants: A generalized two-process model. *J. Mol. Biol. 286*, 607−616.
(60) Woodward, C., Carulla, N., and Barany, G. (2004) Native State Hydrogen-Exchange Analysis of Protein Folding and Protein Motional Domains. In *Methods in Enzymology* (Jo, M., Holt, M. L. J., and Gary, K. A., Eds.) pp 379−400, Academic Press, New York.
(61) Henkels, C. H., and Oas, T. G. (2006) Ligation-state hydrogen exchange: Coupled binding and folding equilibria in ribonuclease P protein. *J. Am. Chem. Soc. 128*, 7772−7781.
(62) Sugase, K., Dyson, H. J., and Wright, P. E. (2007) Mechanism of coupled folding and binding of an intrinsically disordered protein. *Nature 447*, 1021−1025.
(63) Boehr, D. D., Nussinov, R., and Wright, P. E. (2009) The role of dynamic conformational ensembles in biomolecular recognition. *Nat. Chem. Biol. 5*, 789−796.
(64) Wales, T. E., and Engen, J. R. (2006) Partial Unfolding of Diverse SH3 Domains on a Wide Timescale. *J. Mol. Biol. 357*, 1592−1604.
(65) Weis, D. D., Kjellen, P., Sefton, B. M., and Engen, J. R. (2006) Altered dynamics in Lck SH3 upon binding to the LBD1 domain of *Herpesvirus saimiri* Tip. *Protein Sci. 15*, 2402−2410.
(66) Dharmasiri, K., and Smith, D. L. (1996) Mass spectrometric determination of isotopic exchange rates of amide hydrogens located on the surfaces of proteins. *Anal. Chem. 68*, 2340−2344.
(67) Truhlar, S. M. E., Croy, C. H., Torpey, J. W., Koeppe, J. R., and Komives, E. A. (2006) Solvent accessibility of protein surfaces by amide H/^{2}H exchange MALDI-TOF mass spectrometry. *J. Am. Soc. Mass Spectrom. 17*, 1490−1497.
(68) Houde, D., Arndt, J., Domeier, W., Berkowitz, S., and Engen, J. R. (2009) Characterization of IgG1 conformation and conformational dynamics by hydrogen/deuterium exchange mass spectrometry. *Anal. Chem. 81*, 2644−2651.
(69) Monroe, E. B., Kang, S., Kyere, S. K., Li, R., and Prevelige, P. E. (2010) Hydrogen/Deuterium Exchange Analysis of HIV-1 Capsid Assembly and Maturation. *Structure 18*, 1483−1491.
(70) Mohan, A., Oldfield, C. J., Radivojac, P., Vacic, V., Cortese, M. S., Dunker, A. K., and Uversky, V. N. (2006) Analysis of molecular recognition features (MoRFs). *J. Mol. Biol. 362*, 1043−1059.